Jurnal Kejuruteraan 38(2) 2026: 877-886
https://doi.org/10.17576/jkukm-2026-38(2)-31

Numerical Simulation of Pulse Laser-Generated Ultrasonic Wave and Amplitude Peak Count for Defect Detection

Nazirah Ab Wahab[a*], Amelda Dianne Andan[b], Nurhalawa Md Yusof[c] & Chindada Sony[d]

[a]*Faculty of Civil Engineering, Universiti Teknologi MARA,*

40450 Shah Alam, Selangor, Malaysia

[b]*Kuliyyah of Engineering, Department of Mechanical and Aerospace Engineering,*

International Islamic University Malaysia, 53100 Gombak, Malaysia

[c]*Acoustics, Ultrasound & Vibration, Electrical Group,*

National Metrology Institute of Malaysia, 43900 Sepang, Malaysia

[d]*Institute of Thermomechanics of the CAS, v. v. i.,*

Dolejškova 1402/5, 182 00 Praha 8, Czech Republic

[*]*Corresponding author: nazirahwahab@uitm.edu.my*

Received 4 July 2025, Received in revised form 19 October 2025
Accepted 19 November 2025, Available online 30 March 2026

ABSTRACT

High spatial resolution and the possibility for distant and noncontact measurements have led to substantial research into laser ultrasonic techniques. Pulse lasers produce heat when the surface of a target object absorbs its electromagnetic energy. When a material undergoes a temperature shift, it generates stress and strain fields, which in turn cause an elastic wave known as ultrasound. This research simulated the effects of an ultrasonic wave produced by a laser striking an aluminium plate. Using extremely fine meshes, the pulse laser stimulation is modelled as a localised heat flux imposed to the structure's surface. The 2D simulation data for intact specimen is collected and then compared to an existing experimental data using contactless laser ultrasonic measuring equipment . The model is then subjected to surface damage and identified using a threshold to retrieve the peak count from the laser ultrasonic data while analysing the correlation between damage effects found in various locations and peak counts. The total number of peak counts is measured, and the damage is successfully detected. Based on the identified peak counts, different damage locations can be determined and analysed.

Keywords: Laser ultrasonics; finite element method; damage localization; peak count

INTRODUCTION

Non-destructive testing has experienced substantial growth in engineering applications that evaluate the reliability of materials (Yang et al. 2024; Xu et al. 2023; Zhang et al. 2022; Yi et al. 2019). This growth has been fueled by the rising demand for precise, efficient, and sustainable testing methodologies in industries like aerospace, automotive, and civil engineering. As technology has advanced, laser ultrasonic analysis has become a promising non-destructive alternative (Wang et al. 2023; Fu et al. 2024). The technology is recognized for its high accuracy and ability to detect minute defects that may go unnoticed using conventional methods. This technology has considerable potential due to its contactless, wide-band, rapid, and great sensitivity capabilities (Zhang et al. 2024; Fu et al. 2024). These features enable its application in environments where traditional contact-based methods would be impractical or hazardous.

Not only is it appropriate for remote tracking in harsh conditions, but it can also be employed for the online, real-time examination of micro-cracks (Li et al. 2025; Liu et al. 2016). This capability is especially relevant in safety-critical structures, such as bridges and aircraft, where early detection of micro-cracks can prevent catastrophic failures.

During the ultrasonic signal transmission through a medium with fissures, three distinct types of waves are produced, including reflection, transmission, and mode conversion. These waveforms provide critical insights into the type, size, and location of defects within the material. Monitoring the transmission waveform or reflection of the fracture can assess the defect data present in the sample (Chen et al. 2022).

Early researchers employed numerical simulation for assessing laser ultrasonic identification via the thermoelastic process. In an effort to resolve the thermoelastic issue, the effects of pulse width and spot radius on ultrasonic signal generation were assessed and described as a 2D theoretical model (Arias et al. 2003). Subsequent studies explored the influence of laser pulse duration, frequency, and energy on signal clarity and amplitude. Different research looked at the displacement and temperature data for measuring the thickness of an aluminum plate using ultrasonic techniques (Liu et al. 2016). Further investigations revealed that optimizing laser pulse characteristics could improve signal-to-noise ratio and enhance detection sensitivity. In addition, the function of laser pulses with limited spatial and temporal forms was investigated, as was the impact of heat diffusion on the formation of elastic waves in non-metallic materials (Wang et al. 2007). Further study explored the relationship between the pulsed line source laser's half-width and the properties of the displacement signals produced by Rayleigh and Lamb waves (Wang et al. 2007). Rajagopal (Rajagopal et al. 2021) states that the period of the laser pulse and the optical attenuation coefficient both affect acoustic pulses. However, previous studies only focused on the field of displacement, even though the stress field and transient temperature field need consideration as they involve the laser parameters as well as the excitation ultrasound signals.

Laser ultrasonic testing has been increasingly used to detect flaws in recent years. Research by Cavuto created an all-inclusive axle-wheel identifier that uses ultrasonic waves penetrating both solids and air (Cavuto et al. 2021). This innovation illustrates the flexibility of laser ultrasonic testing in multi-material environments. Before experimental confirmation, a mathematical analysis utilizing the finite element method is necessary to understand the physical mechanism of laser ultrasonic detection. This analytical approach allows for the prediction of wave behavior under varying conditions, such as material heterogeneity and defect orientation. Several scholarly investigations have focused on numerically simulating angled surface fractures using laser ultrasonic technology (Han et al. 2022; Wang et al. 2023; Li et al. 2022). Dutton demonstrated that the reflection and transmission coefficients are associated with the length and angle of the defect based on studies conducted using the finite element technique (Han et al. 2022). Zeng found the inclination of surface cracks by looking at the spectra and amplitudes of Rayleigh waves (Zeng et al. 2019). In addition, a technique to quantitatively identify surface-breaking fissures by fitting the Rayleigh wave's reflection and transmission coefficients also investigated. According to Wang's demonstration (Wang et al. 2021), the peak-to-valley variance of the Rayleigh echo is linearly related to the depth of the fracture. This discovery underpins many modern inspection protocols for subsurface defect detection. The technique for quantitatively evaluating surface-angled damages was also established by Han (Han et al. 2022).

This research goal is to boost knowledge of laser ultrasonic testing as a non-destructive evaluation technique. While prior research has shed light on topics such as the thermoelastic mechanism, the influence of laser settings on ultrasonic signal analysis, and mathematical modeling using the finite element technique, this work seeks to bring a fresh perspective to the relevant subject. This research further aims to identify damage independently of any reference data from the undamaged condition, which is a significant advancement in the field of ultrasonic testing. The findings are expected to enhance current detection methodologies and contribute to the development of smart inspection systems capable of autonomous flaw detection in critical infrastructure.

THEORETICAL BACKGROUND

LASER-GENERATED ULTRASONIC WAVE

The electromagnetic radiation emitted by a pulse laser can be absorbed by solid surfaces when the laser is pointed at them. This could potentially lead to localised heating. In cylindrical coordinates, the resultant thermal diffusion can be expressed as follows (Liu et al. 2016):

$$\rho C_p \frac{\partial T(r,z,t)}{\partial t} = \nabla\left(k\nabla T(r,z,t)\right) + Q \tag{1}$$

In this equation, the distribution of temperatures at time t is denoted by T(r,z,t), where r is a radial vector and z is a depth vector. represents the density, while and denote the specific heat capacity at a constant pressure, and thermal conductivity respectively. One definition of Q is the heat source's power density (Liu et al. 2016). Since the pulse laser is not considered a heat source but rather a heat flow, Equation (1) can be simplified to:

$$\rho C_p \frac{\partial T(r,z,t)}{\partial t} = \frac{1}{r}\frac{\partial}{\partial r}\left(rk\frac{\partial T(r,z,t)}{\partial r}\right) + \frac{\partial}{\partial z}\left(k\frac{\partial T(r,z,t)}{\partial z}\right) \tag{2}$$

The natural boundary conditions for laser energy absorption are outlined as follows:

$$-k\frac{\partial T(r,z,t)}{\partial z}|_{z=0} = If(r)g(t),\ \frac{\partial T(r,z,t)}{\partial z}|_{z=h} = 0 \quad (3)$$

In the equation, represents the absorbed laser beam's power intensity, describes its spatial distribution, and is the pulse laser beam's time-based distribution. The top surface is at =0, and the bottom surface is at (Figure 1). indicates the specimen's thickness. Thermal waves carry the heat from the heating process to the specimen. Material stresses and strains are generated in the specimen as a result of thermal expansion within the heated zone. Stress redistribution across the equation is caused by elastic waves (ultrasound), which are generated by a sudden shift in stress in a specific location of the specimen (Liu et al. 2016):

$$(\lambda + 2\mu)\nabla(\nabla . U(r,z,t)) - \mu\nabla \times \nabla \times U(r,z,t) - \alpha_t(3\lambda + 2\mu)\nabla T(r,z,t) = \rho\frac{\partial^2 U(r,z,t)}{\delta^2 t} \quad (4)$$

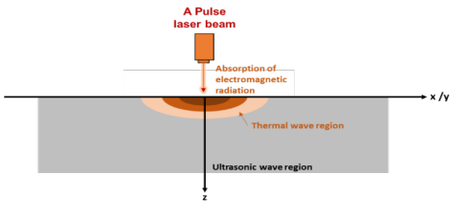

FIGURE 1. Description of the ultrasonic wave

PEAK COUNT

Velocity signal peak counts provide information on wave characteristics and damage status. Velocity signals from intact areas or structures often show consistent peak counts. When there is damage, the peak counts could change due to wave reflections, dispersion, and mode conversions. Hence, at various sensing points, the peak frequencies in the velocity patterns obtained from the perfect specimen and the damaged specimen are compared. Contrasting peak counts might show inconsistencies or outliers, which can lead to the identification of damage. The proportion of the total number of peaks (Nt) to the peak number exceeding a specified threshold (T) was used to establish the peak count in this study. The peak count is a function of time when T ranges from 0 to 1.

The peak count plot was constructed using the methodology detailed in the following procedures. It is necessary to first gather the velocity signals from both the intact and damaged specimens at various measurement sites. Second, a "T" value between zero and one was used to establish the threshold number. This cut-off setting defines the minimum visible peak amplitude. Step three involves counting the number of velocity signal peaks that are higher than the threshold value (T). Step four comprises tallying up the velocity signal's peak-to-peak ratio (Nt). The following step is to determine which peak count, out of all the peaks Nt, is greater than the threshold value. Procedures 2 through 5 are repeated with different threshold values (T) between 0 and 1. A slight adjustment was made (e.g., 0.05) to the threshold to track the variation in peak counts and determine the total number of peaks in all thresholds.

NUMERICAL VALIDATION

DESCRIPTION OF NUMERICAL SIMULATION

This research applies a two-dimensional model to simulate a 150 mm radial and 3 mm thick metal plate (Figure 2). The 2D model serves as a simplified yet effective representation of real-world scenarios, enabling an in-depth analysis of wave propagation and interaction with defects. The focal point of a pulse laser beam with a radius of 1 mm applies 10 mJ of energy for a period of 8 ns in the center of the plate. This concentrated laser energy generates thermal stress, which in turn creates ultrasonic waves that travel through the plate's structure. The model is segmented into the heat wave and the ultrasonic wave zones, to simulate the various physical processes that take place once the laser beam hits the plate (Liu et al. 2016). This dual-zone approach allows for the analysis of the coupled thermal and elastic effects that influence wave behavior.

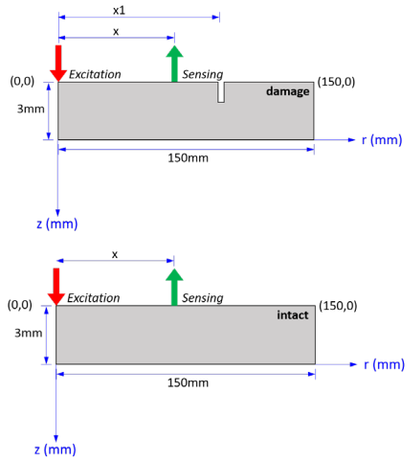

FIGURE 2. Laser irradiating plate schematic based on a 2D finite element model (cross-section drawn) for intact and damaged specimens

TABLE 1. Properties of the specimen

Density, ρ (kg/m^3)	Elastic modulus, E (GPa)	Poisson's ratio, υ	Thermal conductivity k (W/(m·K))	Heat capacity C_p (J/(kg.K))	Thermal expansion Coefficient	Reflection coefficient R_c
2700	68.9	0.33	170	900	2.34 x 10^{-5}	0.95

Assessing the ultrasonic waves using thermoelasticity involves modeling the thermal stress caused by the pulse laser. The rapid temperature rise due to laser energy absorption induces localized expansion, creating stress waves that propagate through the material. The second step is to use elastic wave analysis to mimic the passage of ultrasonic waves through the materials. Elastic wave propagation analysis considers the mechanical behavior of the material, including displacement, velocity, and stress fields. Triangular elements are used to mesh the model, and hierarchical elements are employed to minimize the simulation strain. The use of triangular elements allows for the creation of a highly refined mesh, ensuring greater accuracy in the simulation of wave behavior and interactions.

Damage to the 2D object occurs at the points (x1, 0), where artificial flaws are introduced to represent real-world defects. The dimensions used for the damage simulation are 0.2 mm in width and 0.5 mm in length. This controlled damage size facilitates the investigation of defect detection sensitivity and accuracy. Sensor points were placed on the surface of both the damaged and undamaged aluminum sheets at coordinates (x, 0), strategically positioned to capture the reflection, transmission, and mode conversion of the ultrasonic waves. The collected data from these sensor points provide insights into how defects affect the waveforms, offering crucial information for defect characterization. By incorporating multiple sensor locations, the study enables a comprehensive understanding of how the spatial arrangement of defects influences the observed wave responses.

To further refine the accuracy of the numerical simulation, a time-stepping algorithm is implemented to capture transient changes in thermal and elastic wave behavior. This time-dependent approach captures the evolution of waveforms as they propagate and interact with the defect, allowing for a more realistic representation of real-world conditions. The combined thermal and ultrasonic simulation approach provides a holistic understanding of how laser-induced stress waves interact with defects. These insights are critical for improving the design of non-destructive testing methods and advancing defect detection techniques in engineering materials.

The 10 mJ of energy from the pulse laser is applied to the top surface of the plate as a heat flux. Assuming the other barriers are thermally insulated, the top surface is the only one that is accessible to the pulse laser. The internal heat flow operating on the surface boundary is able to be described using Equation (5).

$$I_{in}(r,t) = I_0(1-R_C)\left(\frac{1}{\pi\sigma_r^2}\right)e^{-\left(\frac{r^2}{2\sigma_r^2}\right)}g(t) \quad (5)$$

Where represents the maximum power of the pulse laser, and is the reflection coefficient of the aluminium plate surface. The laser beam's power intensity is presumed to follow a Gaussian distribution along the direction, with the standard deviation of the Gaussian laser beam, , is set at 0.3 mm. Presumably, the laser beam's temporal function is a pulse function. Table 1 lists the material properties of the aluminum plate model used in simulating laser-induced in numerical simulations.

NUMERICAL MODEL VERIFICATION

Figures 3 and 4 show the experimental findings of a full noncontact laser ultrasonic system compared to the simulation results, which demonstrating the validity of the proposed model in in this work. A study by Liu (Liu et al. 2016) provides an expanded review of the transmission of ultrasonic waves and experimental production via laser pulses. The experiment's sensing point was 40 mm away from the centroid, while the excitation point was at the centroid itself.

Figure 5 shows the normal out-of-plane velocities observed at a surface sensor on the 1, 2, and 3 mm thick simulated aluminium plates. The experiment is compared with the findings. The simulation velocity data need to be pre-processed through a 350 kHz low-pass filter since that is the highest frequency that the experimental LDV can handle. Moreover, considering energy loss (such as reflection) during the experiment, the specimen's illumination intensity from the laser could vary among the experiments and simulations. Velocity data that has been amplitude-normalised is also shown in Figure 5. Waveforms of velocities obtained through simulations and experiments are comparable.

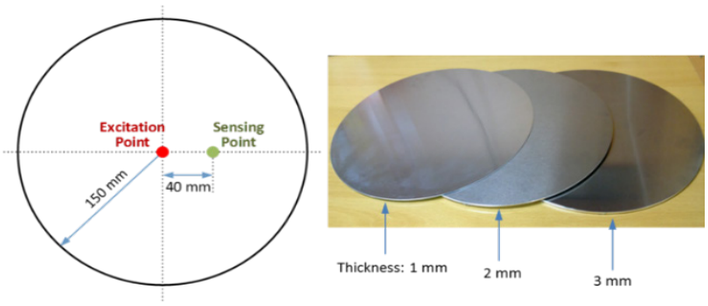

FIGURE 3. Geometric dimensions of the specimens and excitation and sensing point placement (Liu et al. 2016)

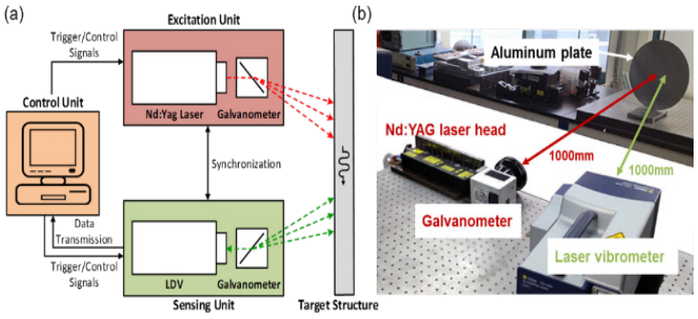

FIGURE 4. Experimental verification: (a) schematic representation for the noncontact laser ultrasonic structure; (b) experiment setup (Liu et al. 2016)

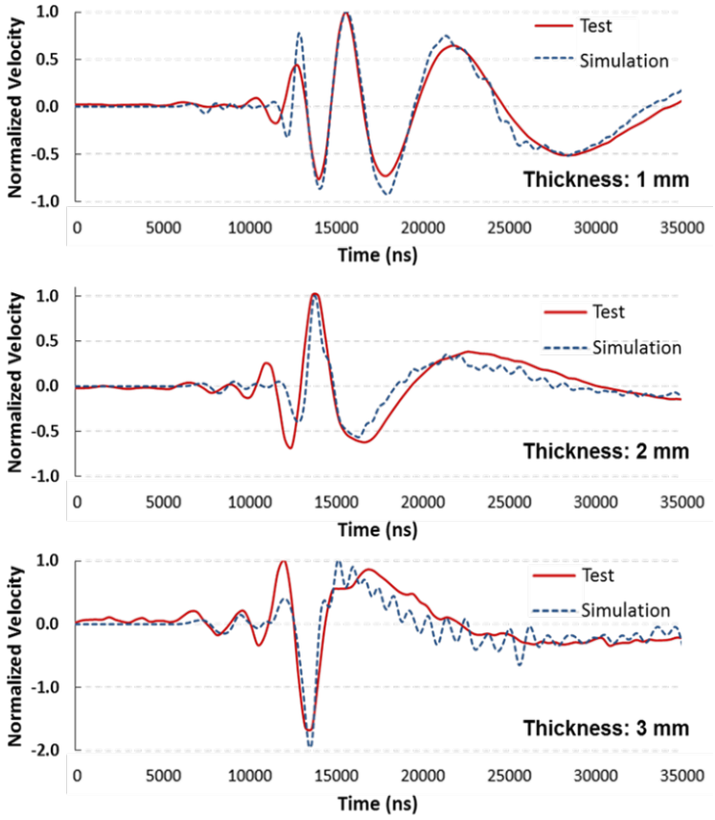

FIGURE 5. Analysis of the velocity indications derived from different thicknesses as measured experimentally (Liu et al. 2016)

RESULTS AND DISCUSSIONS

There are two components to laser-excited ultrasound simulation: thermal physics and mechanical structure. The pulsed laser is pointed to the top surface of the aluminium, where it quickly creates heat. The quick buildup of heat leads to the formation of transient temperature fields. Thermal expansion transfers the heat energy to the metal, creating a momentary stress field. The velocity of the stresses in the stress field provides a quantitative measure of the excitation's effectiveness.

EFFECT OF SENSING POINT PLACEMENT

The ideal placement of sensing points is crucial to the signal measurement. This research investigates the direct and indirect consequences of wave-induced damage. Figure 6 shows the velocity signals that were acquired without damage data. As x = 30, 40, 50, 60, and 70 mm, the sensing point is at coordinates (x, 0). The velocity signals become less significant as the distance between the places of sensing and excitation increases. In other words, the velocity signals become less robust as one moves away from the source of excitation and closer to the point of detection. This behaviour can be explained by the fact that the wave energy is attenuated as it passes through the structure. For example, a direct wave path that is shorter and has minimal energy loss could be accomplished by situating the sensing point 30 mm from the excitation position. A more pronounced rise in the velocity signals is the result. At x = 70 mm, for instance, the direct wave path is longer, and the wave energy experiences more attenuation owing to dispersion and material damping. Consequently, the velocity signals at the sensing location experience a decrease in magnitude.

In addition, Figure 7 demonstrates the observed velocity signals when damage is introduced within (x=50, x=60, and x=70 mm) and beyond (x=30, and x=40 mm) the direct path. The results show that even when the damage is not along the path of the waves themselves, reflections from the damage cause significant alterations in the measured signal compared to the pristine condition. Strong interactions and scattering effects occur when damage is induced inside the direct wave propagation path (such as at x=50, x=60, and x=70 mm). Significant variations in the recorded velocity signals at the sensing site are caused by the additional reflections, refractions, and mode conversions due to these interactions. Damage prevents the waves from travelling smoothly, leading to distorted and altered signals during measurements. However, the waves still indirectly interact with the damaged region when it is located beyond the direct wave path (for example, at x=30 and x=40 mm). After traveling along the direct path, the waves are reflected and dispersed when they come into contact with the damage. These reflected waves travel back through the structure's intact parts before reaching the sensing location. Indirect interactions nonetheless result in detectable shifts in the observed velocity signals but to a lower extent than when the damage occurs along the direct path.

The velocity signals of an intact specimen are shown in Figure 6, while those of a damaged specimen are shown in Figure 7. A wave can only continue its path unimpeded if the number of peaks in the velocity signals measured at different sensing sites is very close to one another (Figure 6). The number of peak counts can be analysed to observe the impact of damage on wave behaviour, whether it is introduced outside or inside the direct propagation route of a wave. Damage alters the properties of wave propagation, increasing scattering, reflections, or mode conversions, as shown by variations in peak counts between damaged and intact specimens.

DAMAGE LOCALIZATION BASED ON NUMBER PEAK COUNTS GENERATED BY LASER ULTRASONIC WAVES

Figure 8 demonstrates the velocity signals that were normalised and obtained from the damaged specimen at the x=50 mm location. The figure shows the normalised velocity signal as a curve along the r-axis for each sensor site. An application of the Fast Fourier Transform (FFT) was made to change the ultrasonic data acquired from the damage case into the frequency domain. The amplitudes of the frequency-domain emissions were brought down to a single reference range by a standardisation process. This makes it possible to compare the amplitudes of signals or sensor points on a regular basis. Additionally, the figure displays the normalised frequency-domain signals at several sensor locations for the damaged casing. Peak counting is carried out at each sensor point using threshold values between 0.1 and 1, with a 0.05 increment. The corresponding peak for each threshold value between 0.1 and 1 was rounded to the closest 0.05. For each threshold value, the sum of all peaks is calculated by counting the peaks that are higher than the threshold. The entire method is repeated with a variety of sensing point locations to enable a spatial analysis of the peak counts.

Figure 9 shows the total number of normalised peak counts for the damage at x=50 mm, and Figure 10 shows the same data for x=80 mm, two different sensor sites. A linear regression model with a 95% confidence range was included with every damage setting. The dataset that corresponds to the damage site at x=50 mm and starts at point 7 (50, 0) is an outlier since it differs significantly from the overall data pattern.

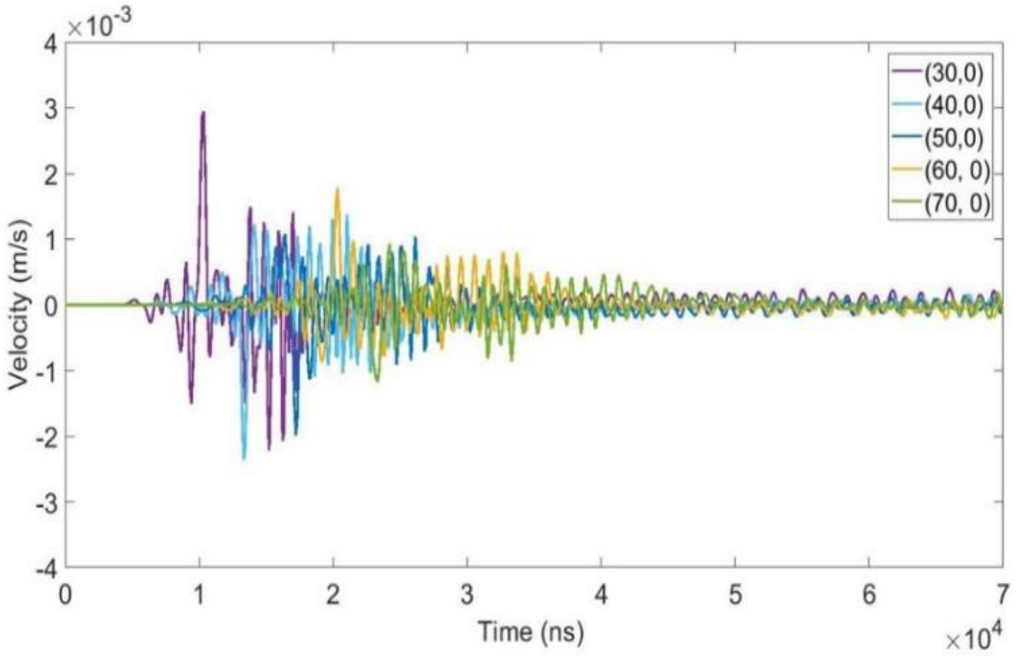

FIGURE 6. Velocity signals obtained from the intact specimen at varying sensing point locations (x, 0)

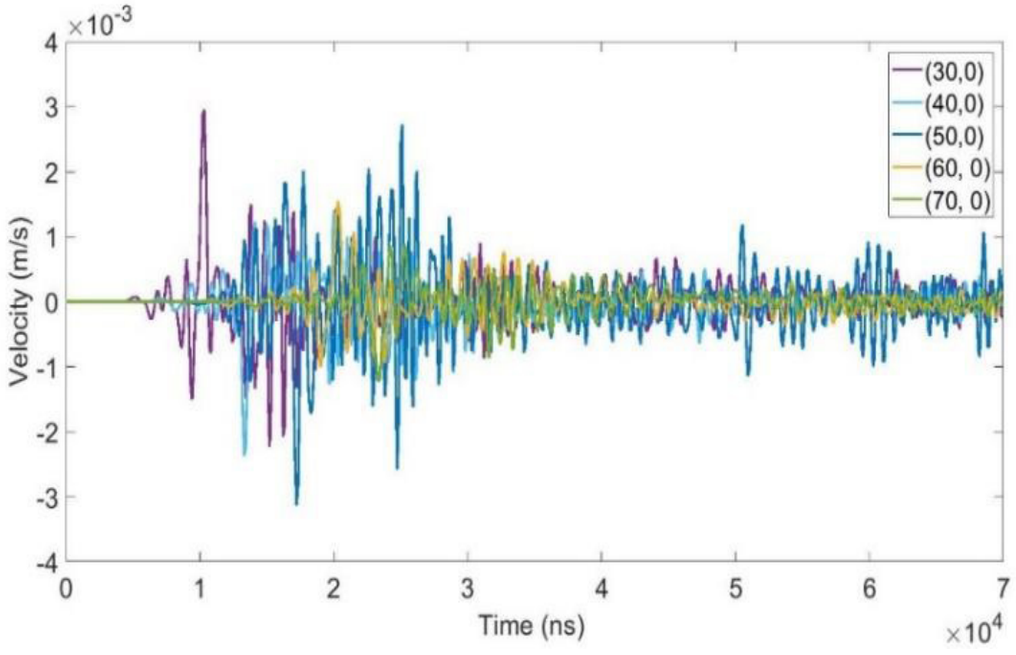

FIGURE 7. Velocity signals obtained from the damaged specimen at varying sensing point locations (x, 0)

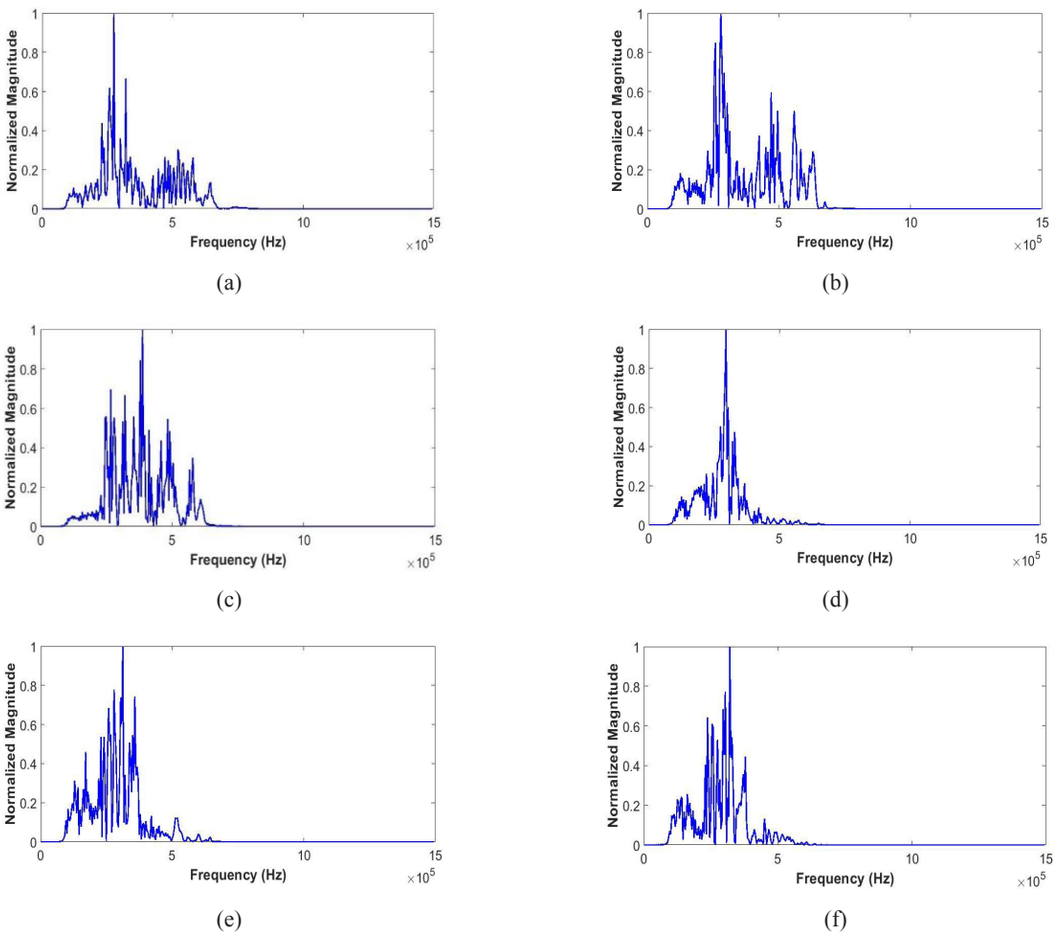

FIGURE 8. Normalised velocity signals obtained from the damaged specimen at varying sensing point locations (x, 0) where (a) x =30mm, (b) x =40mm, (c) x = 50mm, (d) x = 60mm, (e) x =70mm, (f) x = 80mm respectively

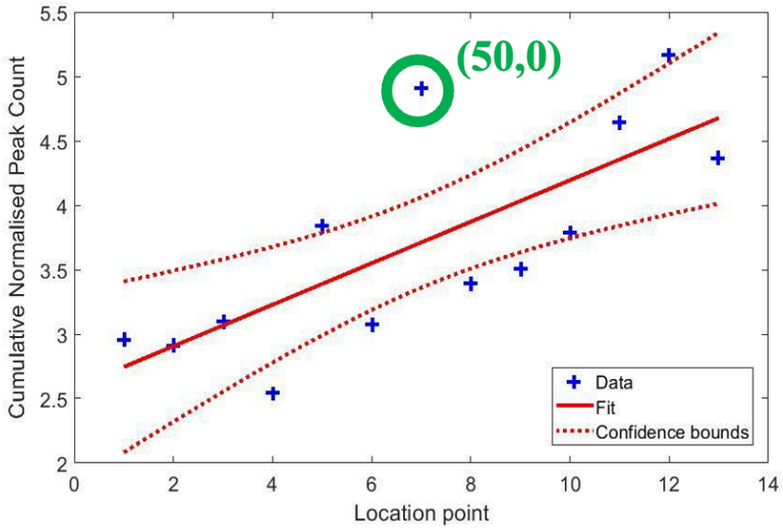

FIGURE 9. Linear model fitting for specimen with damage located at (50, 0)

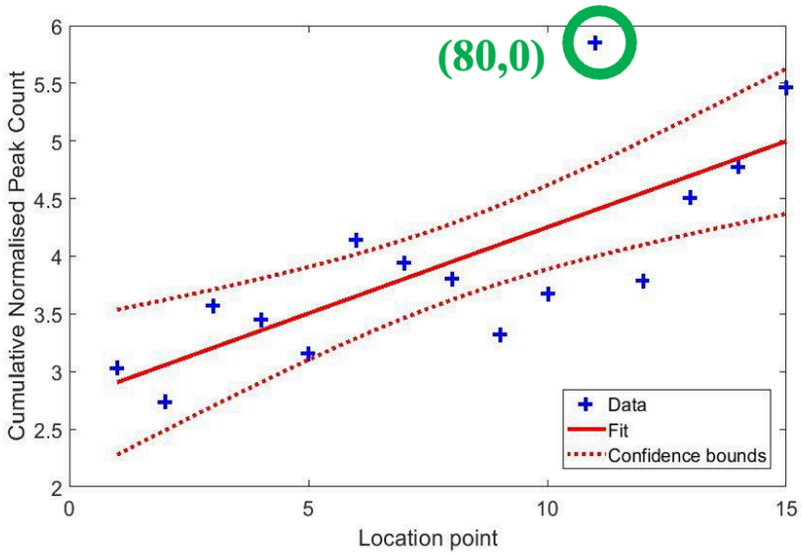

FIGURE 10. Linear model fitting for specimen with damage located at (80, 0)

CONCLUSION

This study presents a new method for laser ultrasonic damage localisation by employing frequency-domain analysis of ultrasonic responses. The model for the simulation is split into two halves, one for thermal waves and the other for ultrasonic waves, to facilitate efficient calculation. Previous work by Liu (Liu et al. 2016) on aluminium plates validates the effectiveness of the simulation model, which correlates well with the experimental findings. Damage is subsequently incorporated into the model, and the peak count of velocity signals in the frequency domain is extracted to facilitate damage visualisation. The study provides a practical approach to quantitative damage assessment. It is beneficial to reduce detection evaluation duration and allow for the implementation of laser ultrasound identification without requiring accurate baseline data.

ACKNOWLEDGEMENT

The authors extend their gratitude to the Universiti Teknologi MARA for providing support through the Geran Penyelidikan MyRA 600-RMC/GPM LPHD 5/3 (009/2023).

DECLARATION OF COMPETING INTEREST

None.

REFERENCES

Arias, I., & Achenbach, J. D. 2003. Thermoelastic generation of ultrasound by line-focused laser irradiation. *International Journal of Solids and Structures* 40(25): 6917–6935.

Cavuto, A., Martarelli, M., Pandarese, G., Revel, G., & Tomasini, E. 2021. FEM based design of experiment for train wheelset diagnostics by laser ultrasonics. *Ultrasonics* 113: 106368.

Chen, C., Sun, A.Y., Ju, B.F., & Wang, C.Y. 2022. Width and depth gauging of rectangular subsurface defects based on all-optical laser-ultrasonic technology. *Applied Acoustics* 191: 108684.

Fu, L.L., Wu, J.H., Yang, J.S., Li, S. & Wu, Z. 2024. Laser ultrasonic damage identification of composites based on empirical mode decomposition and neural network. *Optics and Lasers in Engineering* 181: 108397.

Han, S., Lian, Y., Xie, L., Hu, Q., Ding, J., Wang, Y. & Lu, Z. 2022. Numerical simulation of angled surface crack detection based on laser ultrasound. *Frontiers in Physics*, 10: 982232.

Li, H., Cui, L., He, D., Shi, Z., Bu, F., Cao, Q. & Wan, S. 2025. Effect of ultrasonic-assisted laser metal deposition on microcracks in deposition layer. *Optics and Lasers in Engineering* 181(A): 111747.

Li, H., Liu, Y., Deng, J., An, Z., & Pan, Q. 2022. Depth and angle evaluation of oblique surface cracks using a support vector machine based on seven parameters. *Applied Sciences* 12(16): 8124.

Liu, P., Nazirah, A.W. & Sohn, H. 2016. Numerical simulation of damage detection using laser-generated ultrasound. *Ultrasonics* 69: 248-258.

Rajagopal, S. & Cox, B.T. 2021. Modelling laser ultrasound waveforms: The effect of varying pulse duration and material properties. *The Journal of the Acoustical Society of America* 149(3): 2040-2054.

Wang, C., Yang, D., Lu, K., Wang, W., Chen, Z., Chen, Y., & Ju, B.F. 2024. Laser-generated surface waves for quantitative detection of inclined surface cracks based on finite element analysis. *Nondestructive Testing and Evaluation* 39(3): 687-700.

Wang, J., Shen, Z., Xu, B., Ni, X., Guan, J. & Lu, J. 2007. Numerical simulation of laser- generated ultrasound in non-metallic material by the finite element method. *Optics and Laser Technology* 39(4): 806–813.

Wang, Y., Han, S., Yu, Y., Qi, X., Zhang, Y., Lian, Y. & Lv, Z. 2021. Numerical simulation of metal defect detection based on laser ultrasound. *IEEE Photonics Journal* 13(4): 1–9.

Xu, J., & Xu, Z. 2023. Advanced non-destructive testing techniques on materials. *Materials* 16(4): 2934.

Yang, Q., Zhang, Z., Wang, H., Qin, F., & Peng, X. 2024. Applications of non-destructive testing technologies in materials or engineering. *Applied Sciences* 14(5): 1129.

Yi, D.C., Pei, C. X., Liu, T.H. & Chen, Z.M. 2019. Inspection of cracks with focused angle beam laser ultrasonic wave. *Applied Acoustics* 145: 1-6.

Zhang, J., Zhao, X., Yang, B., Li, J., Liu, Y. & Ma, G. 2022. Non-destructive evaluation of porosity in additive manufacturing by laser ultrasonic surface wave. *Measurement* 193: 110944.

Zhang, Y., Zhou, H., Yao, R. & Wu, M. 2024. A laser ultrasonic intelligent inspection method for metal surface defects based on digital twin model. *Measurement* 237: 115219.